

Thermal Decoherence and Disorder Effects on Chiral-Induced Spin Selectivity

Elena Díaz,^{*,†,‡} Francisco Domínguez-Adame,[†] Rafael Gutierrez,^{‡,§,||} Gianauelio Cuniberti,^{‡,§,||} and Vladimiro Mujica[⊥]

[†]GISC, Departamento de Física de Materiales, Universidad Complutense, E-28040 Madrid, Spain

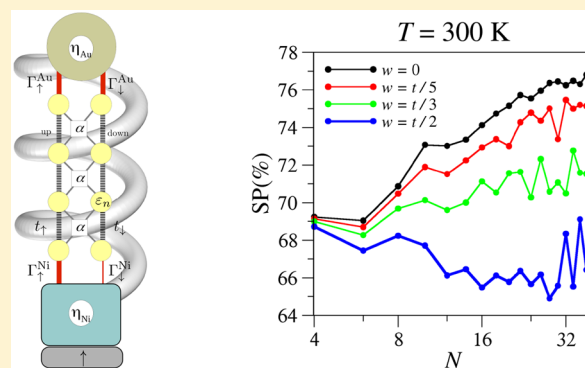
[‡]Institute for Materials Science, TU Dresden, 01062 Dresden, Germany

[§]Dresden Center for Computational Materials Science, TU Dresden, 01062 Dresden, Germany

^{||}Center for Advancing Electronics Dresden, TU Dresden, 01062 Dresden, Germany

[⊥]School of Molecular Sciences, Arizona State University, Tempe, Arizona 85287, United States

ABSTRACT: We use a nonlinear master equation formalism to account for thermal and disorder effects on spin-dependent electron transport in helical organic molecules coupled to two ideal leads. The inclusion of these two effects has important consequences in understanding the observed length and temperature dependence of spin polarization in experiments, which cannot be accounted for in a purely coherent tunneling model. Our approach considers a tight-binding helical Hamiltonian with disordered onsite energies to describe the resulting electronic states when low-frequency interacting modes break the electron coherence. The high-frequency fluctuating counterpart of these interactions, typical of intramolecular modes, is included by means of temperature-dependent thermally activated transfer probabilities in the master equation, which lead to hopping between localized states. We focus on the spin-dependent conductance and the spin-polarization in the linear regime (low voltage), which are analyzed as a function of the molecular length and the temperature of the system. Our results at room temperature agree well with experiments because our model predicts that the degree of spin-polarization increases for longer molecules. Also, this effect is temperature-dependent because thermal excitation competes with disorder-induced Anderson localization. We conclude that a transport mechanism based on thermally activated hopping in a disordered system can account for the unexpected behavior of the spin polarization.



Chiral-induced spin selectivity (CISS) is an intriguing physical effect, first experimentally demonstrated in 1999, that manifests itself as spin-dependent transport in helical, albeit nonmagnetic, molecules.^{1–3} Despite the large amount of experimental^{4–16} and theoretical^{17–32} work published so far, the ultimate origin of the CISS effect is still subject to debate. There seems to be, however, agreement that a combination of the helical conformation of the molecule, together with field and exchange effects, leads to an enhanced spin–orbit interaction that ultimately is responsible for the spin-dependent transmission of electrons in media without time-reversal symmetry. In the specific case of transport experiments,^{3,7,9} an important additional issue is to clarify what the dominant transport regimes are. The majority of the theoretical work previously cited relies on coherent tunneling transport, although attempts to go beyond by introducing decoherence effects^{18,23–25} or leakage of electrons from the molecule to the environment²⁷ have been presented. Additionally, how the length dependence of the spin polarization varies depending on the charge transport regime (coherent or

incoherent) and how important disorder and decoherence are to understand this behavior is also an open issue. Experimentally, photoemission results reported in ref 2 clearly showed a linear increase in the spin polarization with the number of basepairs in dsDNA, up to 80 base pairs. This remarkable behavior, which cannot be explained by a conventional coherent tunneling mechanism that would correspond to an exponential decay of the transmission with increasing distance, is further supported by experiments performed on electrochemical cells with α -helix oligopeptide molecules.¹¹

In this work, we address the length and temperature dependence of the spin polarization in helical molecules using a nonlinear master equation approach within a tight-binding description of the electronic part including spin–orbit interaction.^{20,23} In contrast with previous theoretical inves-

Received: July 13, 2018

Accepted: September 13, 2018

Published: September 13, 2018

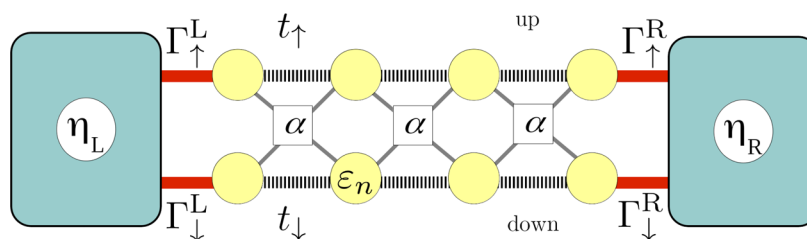


Figure 1. Planar sketch of the helical molecule attached to two ideal leads. The parameters of the tight-binding Hamiltonian and the electronic and the spin–orbit couplings between neighboring sites are shown.

tigations, in the nonlinear master equation description, we include the coupling to high-frequency vibrational degrees of freedom in the form of temperature-dependent transition probabilities between electron states. Additionally, static Anderson diagonal disorder is used to mimic the influence of low-frequency vibrations. This gives rise to a controllable degree of localization of the eigenstates and allow us to deal with thermally assisted transport as well as with coherent propagation in the quasi-resonant tunneling regime. For low or moderate magnitudes of the disorder, our results at room temperature agree qualitatively with the experiments, showing an increase in the spin polarization with the molecular length. This behavior can be inverted, however, in the regime of strong disorder or at very low temperatures. Our results strongly hint at the possibility that a transport mechanism based on thermally activated hopping may be responsible for the unexpected experimentally observed length dependence of the spin polarization.

Our starting point is the tight-binding Hamiltonian derived by Gutierrez et al.,²⁰ which reduces to that proposed by Guo et al.²³ in the limit of a purely radial component of the helical electric field and only a single electronic level per site. Helical symmetry is included by using the appropriate representation of the Pauli matrices in cylindrical coordinates, defining the radius and the pitch of the helix. The Hamiltonian reads

$$\mathcal{H} = \sum_{n=1}^N \varepsilon_n c_n^\dagger c_n + \sum_{n=1}^{N-1} [c_n^\dagger \tau c_{n+1} + i\alpha c_n^\dagger (\sigma_n + \sigma_{n+1}) c_{n+1} + \text{H.c.}] \quad (1)$$

where $c_n^\dagger = (c_{n\uparrow}^\dagger, c_{n\downarrow}^\dagger)$ and $c_n = (c_{n\uparrow}, c_{n\downarrow})^T$ are the electronic creation and annihilation operators at site n of a helical molecule of length N . Here the superscript T refers to transpose and H.c. stands for Hermitian conjugate. The effective spin–orbit coupling constant α and the electronic intersite hopping considered within the matrix $\tau = \text{diag}(t_\uparrow, t_\downarrow)$ will be taken as uniform along the molecule. Notice that we will, in general, assume that these electronic couplings may be spin-dependent. The last term is expressed as a function of the Pauli matrices $\sigma_{x,y,z}$ as follows, $\sigma_{n+1} = \sigma_z \cos \theta + \sin \theta [\sigma_x \sin(n\Delta\varphi) - \sigma_y \cos(n\Delta\varphi)]$, where θ is the helix angle and $\Delta\varphi$ refers to the twist angle between neighboring sites along the helix.²³ Hereafter, $\theta = 0.66$ rad and $\Delta\varphi = \pi/5$ will be considered as typical values for DNA molecules, corresponding to 10 sites per turn. Figure 1 presents a planar view of the helical molecule, indicating the various spin-dependent couplings between neighboring molecular sites.

Electron transport in molecules may be affected by the motion of the constituent ions as well as the possible counterion atmosphere around it. Stochastic fluctuations of the ions cause loss of coherence and energy dissipation. These

random fluctuations often present different time scales, depending on the origin of the molecular vibrations. For instance, intramolecular modes occur at high frequency due to the stretching of stiff covalent bonds, while intermolecular modes span a wide range of frequencies. The coupling of electrons with high-frequency modes will later be accounted for by appropriate transition rates within a nonlinear master equation approach. The influence of low-frequency modes, on the contrary, will be described by the Anderson model of disorders,³³ assuming that onsite energies, ε_n , in eq 1 are random variables given as $\varepsilon_n = \varepsilon + \Delta\varepsilon_n$ with uniform probability distribution:³⁴ $P(\Delta\varepsilon_n) = (1/2w)\Theta(w - \Delta\varepsilon_n)$, where Θ is the Heaviside step function and w is the half-width of the distribution. This parameter will be referred to as magnitude of disorder hereafter. This approximation can be well justified by assuming that the time scales of low-frequency modes are much longer than typical electronic time scales for propagation, so that the electron will see a static, although disordered, energy profile. Although disorder can also be introduced in the electronic coupling matrix elements, we limit ourselves to discuss the simpler case of Anderson onsite disorder.

Notice that, in a similar way as for a 1D lattice, the localization properties of a helical tight-binding model with spin–orbit coupling will sensitively depend on the magnitude of disorder. It is well known that strong disorder localizes the electronic states in regions shorter than the system size, suppressing coherent transport along the system. However, there also exist fast ionic fluctuations that cannot be captured by the static approach. In such a case, electron–vibration coupling can result in thermally activated hopping between localized states of different energy, giving rise to incoherent transport.

Our approach to describe thermally activated transport is based on the calculation of the transition rates between all eigenstates of the Hamiltonian (eq 1), $|\Psi_\mu\rangle$ which fulfill the Schrödinger equation $\mathcal{H}|\Psi_\mu\rangle = E_\mu|\Psi_\mu\rangle$, with $|\Psi_\mu\rangle = \sum_{n=1}^N \sum_{\sigma=\uparrow,\downarrow} \psi_{n\mu}^\sigma |n\sigma\rangle$, where $|n\sigma\rangle$ refers to the local tight-binding basis for a particular spin state σ at a site n .

The probability per unit time of an electron to be transferred from an eigenstate $|\Psi_\mu\rangle$ (with energy E_μ) to another eigenstate $|\Psi_\nu\rangle$ (with energy E_ν) reads³⁵

$$W_{\mu\nu} = W_0 S(|\Delta E_{\mu\nu}|) F(\Delta E_{\mu\nu}, T) J_{\mu\nu} \quad (2)$$

where $\Delta E_{\mu\nu} \equiv E_\mu - E_\nu$ ($\mu, \nu = 1, 2, \dots, 2N$) and $S(|\Delta E|) = |\Delta E|/t$ is the spectral density with $t = (t_\uparrow + t_\downarrow)/2$.³⁵ Here the constant W_0 stands to characterize the strength of the electron–vibration scattering. Temperature, T , appears as a variable of the function $F(\Delta E, T) = \Theta(\Delta E) + n(\Delta E, T)$, where $n(\Delta E, T) = [\exp(|\Delta E|/k_B T) - 1]^{-1}$ is the occupation number of the vibrational mode of frequency $\Delta E/\hbar$, where k_B is the

Boltzmann constant. The parameter $\mathcal{I}_{\mu\nu}$ accounts for the overlap of the eigenstates $|\Psi_\mu\rangle$ and $|\Psi_\nu\rangle$, and it is calculated as

$$\mathcal{I}_{\mu\nu} \equiv \sum_{n=1}^N \sum_{\sigma=\uparrow,\downarrow} (\psi_{n,\mu}^\sigma)^2 (\psi_{n,\nu}^\sigma)^2 \quad (3)$$

Notice that the condition of detailed balance is fulfilled by the transition rates (eq 2) because $W_{\nu\mu} = W_{\mu\nu} \exp(-\Delta E_{\mu\nu}/k_B T)$.

Now, we will use eq 2 to develop a formalism based on a nonlinear master equation to obtain the main features of spin transport by calculating the population of the eigenstates in the stationary regime and from them the spin-dependent electric current. We thus need to solve the following steady-state master equation for the populations P_μ

$$\frac{dP_\mu}{dt} = \frac{dP_\mu}{dt} \Big|_{\text{mol}} + \frac{dP_\mu}{dt} \Big|_{\text{leads}} = 0 \quad (4)$$

Transitions between electronic eigenstates in eq 4 are described by the following expression³⁶

$$\frac{dP_\mu}{dt} \Big|_{\text{mol}} = \sum_{\nu=1}^{2N} [W_{\nu\mu} P_\nu (1 - P_\mu) - W_{\mu\nu} P_\mu (1 - P_\nu)] \quad (5)$$

Nonlinear terms of the form $P_\nu (1 - P_\mu)$ arise from the Pauli exclusion principle. Additionally, one needs to take into account that the molecule is an open system in contact with electronic reservoirs. This leads to additional terms accounting for the transition rates between the molecule and the electrodes

$$\frac{dP_\mu}{dt} \Big|_{\text{leads}} = \sum_{\sigma=\uparrow,\downarrow} [\Gamma_{\mu\sigma}^L (f_\mu^L - P_\mu) + \Gamma_{\mu\sigma}^R (f_\mu^R - P_\mu)] \quad (6)$$

where $f_\mu^{\sigma,R} = \{1 + \exp[(E_\mu - \eta_{L,R})/k_B T]\}^{-1}$ is the Fermi distribution function at the left (L) and right (R) contacts. $\eta_L = E_F + eV/2$ and $\eta_R = E_F - eV/2$ are the chemical potentials of the left and right contacts, respectively, and E_F is the Fermi energy at equilibrium. $\Gamma_{\mu\sigma}^L$ ($\Gamma_{\mu\sigma}^R$) measures the coupling between the left (right) contact and the eigenstate, μ , for a particular spin projection, σ . By assuming energy-independent couplings to the electrodes (wide-band limit) we obtain $\Gamma_{\mu\sigma}^L = \gamma_L^\sigma |\psi_{1,\mu}^\sigma|^2$ and $\Gamma_{\mu\sigma}^R = \gamma_R^\sigma |\psi_{N,\mu}^\sigma|^2$, where γ_L^σ (γ_R^σ) is the transition rate of an electron with a particular spin state from the left (right) electrode to/from the molecule.

To come closer to the typical experimental situation,³ we will consider different contacts coupled at both molecular edges. For the sake of definiteness, we consider the right contact to be a gold electrode, which displays a similar behavior for spin-up and spin-down polarizations. (We are not addressing here issues related to interfacial spin effects.) The left electrode is assumed to be the spin injector (such as a Ni electrode). In a typical experimental setup, the electrode magnetization is controlled by an external magnet that gives rise to a selective spin injection into the molecule. Therefore, the spin-up current in experiments is measured for a particular Ni magnetization, whereas the spin-down current is obtained for the opposite one. In our model, the parameters that control the spin-state of the injected (extracted) electrons are γ_L^σ (γ_R^σ). Accordingly, to evaluate the spin-up current, we will consider the following set of parameters: $\gamma_R^\sigma = W_0$, $\gamma_L^\uparrow = \gamma_R^\sigma$, and $\gamma_L^\downarrow = \gamma_R^\sigma/10$. On the contrary, spin-down currents will be calculated using $\gamma_R^\sigma = W_0$, $\gamma_L^\downarrow = \gamma_R^\sigma/10$, and $\gamma_L^\uparrow = \gamma_R^\sigma$.

Steady-state solutions to eq 4 are found by an iterative method that guarantees the physical condition $0 \leq P_\mu \leq 1$ such that the differences of populations of each state μ at iteration steps i and $i + 1$ are smaller than a given convergence level: $|P_\mu^{(i+1)} - P_\mu^{(i)}| \leq 10^{-4}$. Thus

$$P_\mu^{(i+1)} = \frac{\sum_\nu^{2N} W_{\nu\mu} P_\nu^{(i)} + \sum_\sigma [\Gamma_{\mu,\sigma}^L (f_\mu^L - P_\mu^{(i)}) + \Gamma_{\mu,\sigma}^R (f_\mu^R - P_\mu^{(i)})]}{\sum_\nu^{2N} (W_{\mu\nu} - W_{\nu\mu}) P_\nu^{(i)} + \sum_\nu^{2N} W_{\nu\mu} + \sum_\sigma \Gamma_{\mu,\sigma}^L + \Gamma_{\mu,\sigma}^R} \quad (7)$$

with $i = 0, 1, \dots$ and an initial ansatz arising from the continuity condition

$$P_\mu^{(0)} = \frac{\sum_\sigma (\Gamma_{\mu,\sigma}^L f_\mu^L + \Gamma_{\mu,\sigma}^R f_\mu^R)}{\sum_\sigma (\Gamma_{\mu,\sigma}^L + \Gamma_{\mu,\sigma}^R)} \quad (8)$$

After evaluating the stationary populations, the total electric current is given by³⁶

$$I(V) = \frac{e}{h} \sum_{\mu=1}^{2N} \sum_{\sigma=\uparrow,\downarrow} \Gamma_{\mu\sigma}^R (f_\mu^R - P_\mu) \quad (9)$$

As noted in previous works,^{37,38} the description of the coherent off-resonance tunneling regime requires solving the master equation in the limit of negligible bridge population. In our case, we are describing transport in a situation where the Fermi energy of the system is close to the molecular band. This allows us to simulate both resonant tunneling and hopping, depending on the temperature and disorder strength. It is also important to emphasize that at low temperatures diagonal disorder localizes the eigenstates and reduces the conductance when the Fermi level lies within the molecular energy spectrum. The opposite behavior (increase in conductance with increased disorder) results when the Fermi level lies outside the molecular spectrum. Disorder also results in near-exponential decay of conductance with length, even in systems that would be resonant in the absence of disorder, but it produces much slower falloff of the conductance with length in systems that would not be resonant.

As a preliminary step, we first analyze the conductance of a linear chain with no spin-orbit coupling ($\alpha = 0$ in eq 1). We are interested in the linear transport regime occurring at very low voltages to obtain information about the conductance of the system G . Therefore, we evaluate the electronic current (eq 9) for a voltage at which only the first resonant channel transport is activated. Notice that the latter is proportional to the magnitude of interest, G . For simplicity, we consider the mean onsite energy as $\varepsilon = 0$, and we use $t_\uparrow = t_\downarrow = t = 50$ meV as a typical value for the electronic coupling in organic molecules. To calculate the conductance, we set the Fermi level at the bottom of the molecular band, $E_F = E_1$, and we consider a voltage such that $eV/2 < \Delta E_{21}$ to guarantee single-channel contact coupling, where ΔE_{21} is the energy difference between the two lowest molecular states (see Figure 2). In this way, the second level can be populated only when $\Delta E_{21} - eV/2 < k_B T$.

The results addressing how the conductance depends on temperature, molecular length, and disorder strength are collected in Figure 3, where the conductance averaged over 2000 realizations of the disorder is shown. In Figure 3a, the conductance, G , as a function of the molecular size, N , is shown on double-logarithmic scale for several magnitudes of

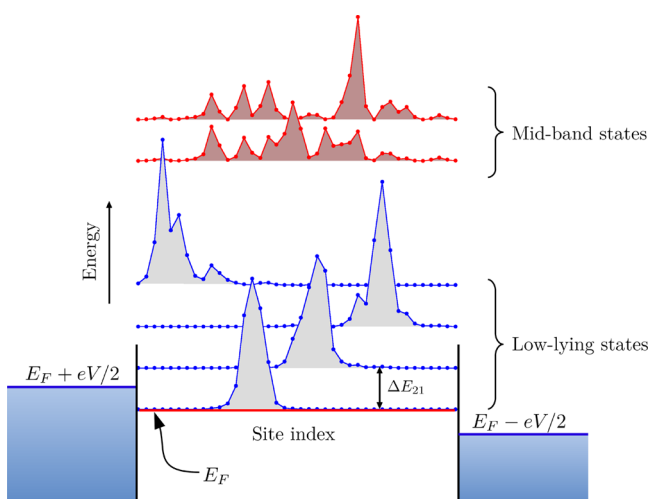


Figure 2. Sketch of the localized eigenstates in a disordered molecule as a function of the site index. Fermi energy, E_F , at equilibrium ($V = 0$) and chemical potentials $E_F \pm eV/2$ in the biased molecule ($V > 0$) are also indicated. The baseline of each state indicates its corresponding energy. States at the bottom of the molecular band are highly localized, whereas the localization length is large for mid-band states. The energy separation between the two lowest states is ΔE_{21} , as indicated in the Figure. The condition $eV/2 < \Delta E_{21}$ ensures that only the ground state is populated at $T = 0$ K.

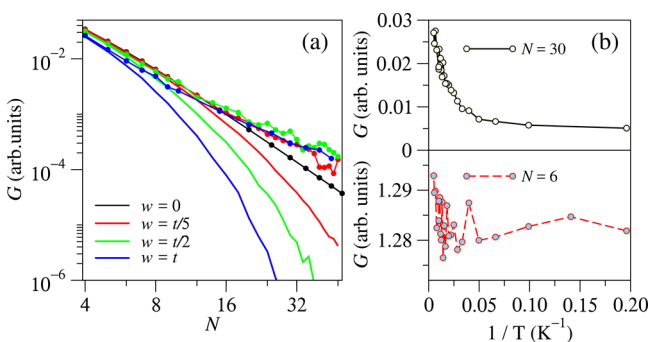


Figure 3. Conductance G as a function of (a) the molecular size N at $T = 0$ K (lines) and $T = 300$ K (lines with solid circles) for different magnitudes of disorder (results at both temperatures in the absence of disorder are the same) and (b) the inverse of temperature for $w = t/5$, $N = 30$ (top panel) and $N = 6$ (bottom panel).

disorder, w , in the system. For the ordered system, all molecular eigenstates are extended, and our results show that G is nearly the same for different temperatures (black lines). In such a case, it is straightforward to obtain an analytical expression for the molecular eigenstates and thus for the electrical conductance. Indeed, our numerical simulations recover such results, showing that the conductance scales as $G \approx N^{-2}$, as expected for nearly resonant tunneling transport.³⁹ If onsite energy disorder is included, the well-known Anderson localization of the eigenstates occurs. Thus the bottom band states display a high degree of localization that is reduced for higher energy states. Indeed, depending on w and N , states with a nonzero probability density to find the particle along the whole molecule may arise. These localization properties have a great impact on the transport properties of the system. At $T = 0$ K (lines), no thermally activated transport can arise, and therefore the conductance is strongly reduced in disordered systems due to the eigenstate localization. Such reduction is

further strengthened when the length of the molecule increases. However, at room temperature $T = 300$ K (lines with solid circles), transitions to higher energy states with a higher spatial extent along the molecule are allowed by the electron–vibration interaction. Therefore, a new mechanism of transport sets in, interstate hopping, and G may reach values similar to those of the ordered system. Remarkably, for short systems, the conductance does not depend on temperature, which accounts for the fact that the localization length is on the order of the system size. The critical molecular length, N^* , at which G becomes temperature-dependent is related to the magnitude of disorder, as expected. In particular, N^* decreases for larger w , which gives rise to a stronger localization of the eigenstates. Therefore, we conclude that for disordered systems the mechanism of thermally activated hopping plays a role when the molecular size is larger than N^* . Figure 3b provides further support to this claim. There, the conductance G as a function of the inverse temperature $1/T$ is shown for a magnitude of disorder $w = t/5$. The top (bottom) panel accounts for results for a molecular size smaller (larger) than the critical one for the considered disorder $N^* \approx 10$. When $N > N^*$, the top panel shows that there is an activation temperature on the order of 25 K within our parameter set, at which thermally activated transport starts playing a role, giving rise to a remarkable increase in G . On the contrary, for small systems such that $N < N^*$, simulations do not show this regime. Therefore, no thermally activated hopping occurs, and the main transport mechanism is due to coherent charge propagation along the extended states in the system.

Let us move to the study of the main features of the electrical conductance and spin polarization in helical systems modeled by the Hamiltonian (eq 1). The theoretical description of spin polarization requires the inclusion of chirality, spin–orbit coupling, and breaking time-reversal symmetry, three ingredients that are present in our model Hamiltonian (eq 1). In particular, the last ingredient is achieved by introducing spin-dependent electronic couplings, $t_{\downarrow} = 2t_{\uparrow} = t = 50$ meV and $\alpha = 5$ meV, while we keep the remaining parameters as in the previous section. In this regard, it is important to stress that within this assumption spin-selectivity arises due to a different transmission probability for spin-up and spin-down electrons, but there is no explicit energy gap between spin-up and spin-down propagating states.

Figure 4 compares the spin-up (-down) conductance, G_u (G_d), at $T = 0$ and 300 K. The plot shows the conductance as a

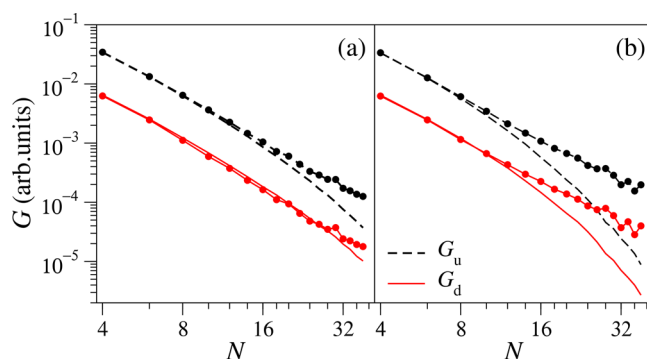


Figure 4. Spin-up (-down) conductance G_u (G_d) as a function of the molecular size N at $T = 0$ K (lines) and $T = 300$ K (lines with solid circles). Different magnitudes of disorder have been considered (a) $w = t/5$ and (b) $w = t/2$.

function of the molecular size for two magnitudes of disorder (a) $w = t/5$ and (b) $w = t/2$. Because of the spin dependency of the electronic couplings, our simulations show that G_u (black dashed lines) $>$ G_d (red solid lines) for all cases. In addition, we recover similar results as those found in Figure 3. If we consider a nonzero temperature (lines with solid circles), thermal effects give rise to a thermally activated transport mechanism, which is responsible for an increase in G_u and G_d . Such thermal activation is more relevant for systems with stronger disorder, where state localization is larger (see Figure 4b).

Last, we focus on the most relevant magnitude in this study, namely, the spin polarization defined as $SP = (G_u - G_d)/(G_u + G_d)$.⁹ In Figure 5, we present the spin-polarization as a function

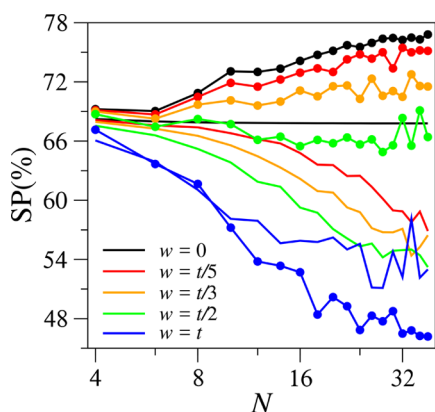


Figure 5. Spin polarization SP(%) as a function of the molecular size N at $T = 0$ K (lines) and $T = 300$ K (lines and solid circles). Different magnitudes of disorder have been considered.

of the molecular size for different magnitudes of disorder at $T = 0$ and 300 K. The inclusion of thermal effects turns out to be crucial to account for the experimental evidence that shows that SP increases with molecular length. At $T = 0$ K, we find that in all considered cases SP decreases as a function of N , as shown by the solid lines in Figure 5. The same effect is found for $T = 300$ K for strong disorder $w = t$. On the contrary, at $T = 300$ K at zero, low, and moderate magnitudes of disorder, we qualitatively reproduce the experimental behavior, namely, SP increasing with N (see the lines with solid circles in Figure 5). It is important to stress that although in our model there is a background spin polarization due to the different electronic couplings for spin-up (t_\uparrow) and spin-down (t_\downarrow) electrons, it becomes almost independent of the molecular length. Therefore, the variation of the SP with the length is directly related to the spin–orbit coupling. Last, if we compare our simulations with previous experimental results for DNA,² we find a slightly lower increase rate of the SP with the molecule length, being on the order of 30% of the measured values for the chosen parameters. A more detailed quantitative comparison is beyond our simplified molecule model, but we still obtain a similar order of magnitude of the effect under consideration. In addition, our numerical results reproduce another expected physical feature, namely, a saturation value of the SP for longer molecules.

In conclusion, we have examined the role of static disorder and thermally induced decoherence on the electron transport regimes in a molecular junction formed by a helical molecule attached to a magnetic (electron injector) and a nonmagnetic

electrode (collector) and the consequences for the length dependence of the spin polarization. Electron–vibration coupling, a key ingredient of decoherence, is implicitly taken into account in the transition probabilities. Depending on the chosen physical conditions (disorder strength and temperature), we are able to describe both resonant tunneling and hopping transport regimes. For the latter one, the most striking result is that for low or moderate disorder strength, the computed spin polarization agrees qualitatively with the observed experimental trend, showing an increasing polarization with molecular length. Thus our results suggest a thermally activated transport regime as a plausible mechanism to explain the experimentally observed length dependence of the spin polarization in the CISS effect.

AUTHOR INFORMATION

Corresponding Author

*E-mail: elenadg@ucm.es.

ORCID

Elena Díaz: 0000-0002-2324-5946

Rafael Gutierrez: 0000-0001-8121-8041

Gianaurelio Cuniberti: 0000-0002-6574-7848

Notes

The authors declare no competing financial interest.

ACKNOWLEDGMENTS

We thank Ron Naaman and Christopher Gaul for very enlightening discussions. This work has been partly supported by Ministerio de Economía y Competitividad–MINECO (Grant MAT2016-75955). E.D. was supported by a José Castillejo postdoctoral fellowship from MINECO. R.G. and G.C. acknowledge financial support from the Volkswagen Stiftung (grant no. 88366). This work was also partly supported by the German Research Foundation (DFG) within the Cluster of Excellence “Center for Advancing Electronics Dresden”. V.M. acknowledges financial support from the DRESDEN Fellowship Programme.

REFERENCES

- (1) Ray, K.; Ananthavel, S. P.; Waldeck, D. H.; Naaman, R. Asymmetric Scattering of Polarized Electrons by Organized Organic Films of Chiral Molecules. *Science* **1999**, *283*, 814.
- (2) Göhler, B.; Hamelbeck, V.; Markus, T. Z.; Kettner, M.; Hanne, G. F.; Vager, Z.; Naaman, R.; Zacharias, H. Spin Selectivity in Electron Transmission Through Self-Assembled Monolayers of Double-Stranded DNA. *Science* **2011**, *331*, 894.
- (3) Xie, Z.; Markus, T. Z.; Cohen, S. R.; Vager, Z.; Gutierrez, R.; Naaman, R. Spin Specific Electron Conduction Through DNA Oligomers. *Nano Lett.* **2011**, *11*, 4652.
- (4) Mishra, D.; Markus, T. Z.; Naaman, R.; Kettner, M.; Göhler, B.; Zacharias, H.; Friedman, N.; Sheves, M.; Fontanesi, C. Spin-Dependent Electron Transmission Through Bacteriorhodopsin Embedded in Purple Membrane. *Proc. Natl. Acad. Sci. U. S. A.* **2013**, *110*, 14872.
- (5) Kiran, V.; Cohen, S. R.; Naaman, R. Structure Dependent Spin Selectivity in Electron Transport Through Oligopeptides. *J. Chem. Phys.* **2017**, *146*, 092302.
- (6) Mondal, P. C.; Fontanesi, C.; Waldeck, D. H.; Naaman, R. Field and Chirality Effects on Electrochemical Charge Transfer Rates: Spin Dependent Electrochemistry. *ACS Nano* **2015**, *9*, 3377.
- (7) Kiran, V.; Mathew, S. P.; Cohen, S. R.; Hernández Delgado, I.; Lacour, J.; Naaman, R. Helicenes – A New Class of Organic Spin Filter. *Adv. Mater.* **2016**, *28*, 1957.

- (8) Michaeli, K.; Kantor-Uriel, N.; Naaman, R.; Waldeck, D. H. The Electron's Spin and Molecular Chirality – How are They Related and How do They Affect Life Processes? *Chem. Soc. Rev.* **2016**, *45*, 6478.
- (9) Aragonès, A. C.; Medina, E.; Ferrer-Huerta, M.; Gimeno, N.; Teixidó, M.; Palma, J. L.; Tao, N.; Ugalde, J. M.; Giral, E.; Díez-Pérez, I.; Mujica, V. Measuring the Spin-Polarization Power of a Single Chiral Molecule. *Small* **2017**, *13*, 1602519.
- (10) Kumar, A.; Capua, E.; Kesharwani, M. K.; Martin, J. M. L.; Sitbon, E.; Waldeck, D. H.; Naaman, R. Chirality-Induced Spin Polarization Places Symmetry Constraints on Biomolecular Interactions. *Proc. Natl. Acad. Sci. U. S. A.* **2017**, *114*, 2474.
- (11) Kettner, M.; Göhler, B.; Zacharias, H.; Mishra, D.; Kiran, V.; Naaman, R.; Fontanesi, C.; Waldeck, D. H.; Şek, S.; Pawłowski, J.; Juhaniewicz, J. Spin Filtering in Electron Transport Through Chiral Oligopeptides. *J. Phys. Chem. C* **2015**, *119*, 14542.
- (12) Naaman, R.; Waldeck, D. H. Spintronics and Chirality: Spin Selectivity in Electron Transport Through Chiral Molecules. *Annu. Rev. Phys. Chem.* **2015**, *66*, 263.
- (13) Mtangi, W.; Tassinari, F.; Vankayala, K.; Vargas Jentzsch, A.; Adelizzi, B.; Palmans, A. R. A.; Fontanesi, C.; Meijer, E. W.; Naaman, R. Control of Electrons' Spin Eliminates Hydrogen Peroxide Formation During Water Splitting. *J. Am. Chem. Soc.* **2017**, *139*, 2794.
- (14) Ben Dor, O.; Yochelis, S.; Radko, A.; Vankayala, K.; Capua, E.; Capua, A.; Yang, S.-H.; Baczewski, L. T.; Parkin, S. S. P.; Naaman, R.; Paltiel, Y. Magnetization Switching in ferromagnets by Adsorbed Chiral Molecules Without Current or External Magnetic Field. *Nat. Commun.* **2017**, *8*, 14567.
- (15) Zwang, T. J.; Hürlimann, S.; Hill, M. G.; Barton, J. K. Helix-Dependent Spin Filtering Through the DNA Duplex. *J. Am. Chem. Soc.* **2016**, *138*, 15551.
- (16) Kettner, M.; Maslyuk, V. V.; Nürenberg, D.; Seibel, J.; Gutierrez, R.; Cuniberti, G.; Ernst, K.-H.; Zacharias, H. Chirality-Dependent Electron Spin Filtering by Molecular Monolayers of Helicenes. *J. Phys. Chem. Lett.* **2018**, *9*, 2025.
- (17) Yeganeh, S.; Ratner, M. A.; Medina, E.; Mujica, V. Chiral Electron Transport: Scattering Through Helical Potentials. *J. Chem. Phys.* **2009**, *131*, 014707.
- (18) Medina, E.; López, F.; Ratner, M. A.; Mujica, V. Chiral Molecular Films as Electron Polarizers and Polarization Modulators. *Europhys. Lett.* **2012**, *99*, 17006.
- (19) Gutierrez, R.; Díaz, E.; Naaman, R.; Cuniberti, G. Spin-Selective Transport Through Helical Molecular Systems. *Phys. Rev. B: Condens. Matter Mater. Phys.* **2012**, *85*, 081404.
- (20) Gutierrez, R.; Diaz, E.; Gaul, C.; Brumme, T.; Domínguez-Adame, F.; Cuniberti, G. Modeling Spin Transport in Helical Fields: Derivation of an Effective Low-Dimensional Hamiltonian. *J. Phys. Chem. C* **2013**, *117*, 22276.
- (21) Eremko, A. A.; Loktev, V. M. Spin Sensitive Electron Transmission Through Helical Potentials. *Phys. Rev. B: Condens. Matter Mater. Phys.* **2013**, *88*, 165409.
- (22) Medina, E.; González-Arraga, L. A.; Finkelstein-Shapiro, D.; Berche, B.; Mujica, V. Continuum Model for Chiral Induced Spin Selectivity in Helical Molecules. *J. Chem. Phys.* **2015**, *142*, 194308.
- (23) Guo, A.-M.; Sun, Q.-F. Spin-Selective Transport of Electrons in DNA Double Helix. *Phys. Rev. Lett.* **2012**, *108*, 218102.
- (24) Guo, A.-M.; Díaz, E.; Gaul, C.; Gutierrez, R.; Domínguez-Adame, F.; Cuniberti, G.; Sun, Q.-F. Contact Effects in Spin Transport along Double-Helical Molecules. *Phys. Rev. B: Condens. Matter Mater. Phys.* **2014**, *89*, 205434.
- (25) Guo, A.-M.; Sun, Q.-F. Spin-Dependent Electron Transport in Protein-like Single-Helical Molecules. *Proc. Natl. Acad. Sci. U. S. A.* **2014**, *111*, 11658.
- (26) Michaeli, K.; Varade, V.; Naaman, R.; Waldeck, D. H. A New Approach Towards Spintronics: Spintronics with no Magnets. *J. Phys.: Condens. Matter* **2017**, *29*, 103002.
- (27) Matityahu, S.; Utsumi, Y.; Aharony, A.; Entin-Wohlman, O.; Balseiro, C. A. Spin-Dependent Transport Through a Chiral Molecule in the Presence of Spin-Orbit Interaction and Nonunitary Effects. *Phys. Rev. B: Condens. Matter Mater. Phys.* **2016**, *93*, 075407.
- (28) Caetano, R. A. Spin–Current and Spin–Splitting in Helicoidal Molecules Due to Spin-Orbit Coupling. *Sci. Rep.* **2016**, *6*, 23452.
- (29) Díaz, E.; Gutiérrez, R.; Gaul, C.; Cuniberti, G.; Domínguez-Adame, F. Coherent Spin Dynamics in a Helical Arrangement of Molecular Dipoles. *AIMS Mater. Sci.* **2017**, *4*, 1052.
- (30) Díaz, E.; Albares, P.; Estévez, P. G.; Cerveró, J. M.; Gaul, C.; Díez, E.; Domínguez-Adame, F. Spin Dynamics in Helical Molecules with Nonlinear Interactions. *New J. Phys.* **2018**, *20*, 043055.
- (31) Matityahu, S.; Aharony, A.; Entin-Wohlman, O.; Balseiro, C. A. Spin Filtering in All-Electrical Three-Terminal Interferometers. *Phys. Rev. B: Condens. Matter Mater. Phys.* **2017**, *95*, 85411.
- (32) Gersten, J.; Kaasbjerg, K.; Nitzan, A. Induced Spin Filtering in Electron Transmission Through Chiral Molecular Layers Adsorbed on Metals with Strong Spin-Orbit Coupling. *J. Chem. Phys.* **2013**, *139*, 114111.
- (33) Anderson, P. W. Absence of Diffusion in Certain Random Lattices. *Phys. Rev.* **1958**, *109*, 1492.
- (34) Klotsa, D.; Römer, R. A.; Turner, M. S. Electronic Transport in DNA. *Biophys. J.* **2005**, *89*, 2187.
- (35) Bednarz, M.; Malyshev, V. A.; Knoester, J. Intraband Relaxation and Temperature Dependence of the Fluorescence Decay Time of One-Dimensional Frenkel Excitons: The Pauli Master Equation Approach. *J. Chem. Phys.* **2002**, *117*, 6200.
- (36) Malyshev, A. V.; Díaz, E.; Domínguez-Adame, F.; Malyshev, V. A. Effects of the Environment on the Electric Conductivity of Double-Stranded DNA Molecules. *J. Phys.: Condens. Matter* **2009**, *21*, 33S105.
- (37) Petrov, E. G.; Zelinskyy, Y. R.; May, V.; Hänggi, P. Charge Transmission Through a Molecular Wire: The Role of Terminal Sites for the Current-Voltage Behavior. *J. Chem. Phys.* **2007**, *127*, 084709.
- (38) Kemp, M.; Mujica, V.; Ratner, M. A. Molecular Electronics: Disordered Molecular Wires. *J. Chem. Phys.* **1994**, *101*, 5172–5178.
- (39) Mujica, V.; Kemp, M.; Ratner, M. A. Electron Conduction in Molecular Wires. II. Application to Scanning Tunneling Microscopy. *J. Chem. Phys.* **1994**, *101*, 6856.